

## ARTICLE OPEN



# Where the winds clash: what is really triggering El Niño initiation?

Gian Luca Eusebi Borzelli<sup>1,2</sup>✉ and Sandro Carniel<sup>2</sup>

El Niño–Southern Oscillation (ENSO) is the Earth’s strongest source of year-to-year climate variability, whose center of action, although being in the tropical Pacific, influences the global climate, impacting also security aspects. ENSO is commonly described as an irregular oscillation of the coupled ocean-atmosphere system, which produces an oscillation in the sea surface temperature between a warm (El Niño) and a cold (La Niña) phase induced by internal waves propagating along the equatorial wave-guide and generated by the convergence between high-frequency westerlies and the quasi-stationary easterlies. Here we show that internal, downwelling Rossby and Kelvin waves are regularly formed beneath the Easterly/Westerly Wind Convergence Zone (EWCZ). When the longitude of EWCZ is located east of 175°E, the Kelvin waves formed beneath the EWCZ reach the eastern Pacific boundary and determine an El Niño event and, the more the EWCZ elongates eastwards into the central Pacific, the more the observed El Niño event is classified as severe, suggesting that the position of the EWCZ is an important factor to trigger El Niño. Therefore, we study zonal shifts of EWCZ and show that the EWCZ and the deep atmospheric convection displace zonally in phase with each other and with the Southern Oscillation Index, indicating that the longitude of the clash between Easterlies and Westerlies determines the climate state of the Pacific and triggers the El Niño initiation.

*npj Climate and Atmospheric Science* (2023)6:119; <https://doi.org/10.1038/s41612-023-00445-9>

## INTRODUCTION

El Niño–Southern Oscillation (ENSO) consists in the phenomenon of a zonal redistribution of heat in the tropical Pacific Ocean, which produces an irregular oscillation in the sea surface temperature (SST) between a warm (El Niño) and a cold (La Niña) phase recurring every 2–7 years<sup>1–4</sup>. ENSO originates in the tropical Pacific through interactions between the ocean and the atmosphere, but its environmental and socioeconomic impacts are planetary<sup>5</sup>. It has been for instance demonstrated that changes in the global weather patterns associated with ENSO determine variations in crop yields, production and export prices in major food-producing regions<sup>6</sup>. Associated with these changes, inflation results in an increase in poverty and social disorders, which enhance the probability of local conflicts<sup>7,8</sup>. Therefore, improving ENSO predictability and understanding its teleconnections is, beyond the scientific relevance, an extremely important issue from the socioeconomic point of view. Spurred on by the powerful El Niño events (super-El Niño) that occurred in 1997–1998 and 2015–2016, efforts to understand the causes and consequences of ENSO have been undertaken and have greatly expanded our knowledge of this phenomenon, but still interlinked issues regarding ENSO dynamics, impacts, forecasting, and applications remain unresolved (see e.g., McPhaden et al.<sup>5</sup>).

Our knowledge of ENSO relies upon its oscillatory nature and focuses on the coupling between changes in the depth of the main thermocline, heat content in the surface layer of the water column and oceanic feedback on the zonal wind pattern. In these theories, the subsurface memory of the ocean (i.e., the energy stored in the water column), depends on the depth of the thermocline and the zonal structure of the isothermal surfaces is sustained by the dynamical balance between the fluid internal pressure gradient and easterly winds<sup>1,9</sup>. This process systematically transfers heat westward and “charges” the western part of

the Tropical Pacific, which is then “discharged” through internal equatorial Kelvin waves<sup>10,11</sup>. Some studies have concentrated on equatorial internal waves associated with zonal displacements of the Pacific Warm Pool (WP), a large area of about  $15 \times 10^6$  km<sup>2</sup> of the western tropical Pacific characterized by the warmest waters of the global ocean, with SST higher than 28–29 °C, which leads to deep atmospheric convection<sup>12–17</sup>. Westerly Winds (WW) in the western/central Pacific and Easterly Winds (EW) in the central/eastern Pacific, determine a convergence of water masses at the eastern edge of the WP and, it has been proved that, the eastern border of the WP displaces rigidly in phase with the Southern Oscillation Index (SOI)<sup>18–23</sup>. Picaut and Delcroix<sup>13</sup> concentrated on equatorial wave sequences associated with WP displacements during 1986–1987 El Niño/1988–1989 La Niña and showed that anomalous zonal advection was associated with Kelvin (KW) and Rossby waves (RWs) excited by a succession of local wind events in the western/central tropical Pacific. Although the central role of KW and RW in El Niño generation is largely recognized (see e.g. Santoso et al.<sup>2</sup> and references cited therein), Kang and An<sup>24</sup> observed that KW and RW contributions to changes in the SST compensate each other in the western equatorial Pacific, while in the eastern equatorial Pacific, the SST variation is primarily due to KW.

Consequently, a systematic investigation about the lateral displacements of the Easterly/Westerly Wind Convergence Zone (EWCZ) is important to potentially better understand and predict ENSO. Indeed, previous studies have indicated that the intensity, location, and timing of WW events are crucial for El Niño development (e.g.<sup>25–27</sup>). Other studies have concentrated on the importance of EW<sup>28–31</sup>. Here, we introduce the longitude of the EWCZ as a synthetic parameter that summarizes the collective action of intensity and location of WW events and EW anomalies. We define the EWCZ as the region where the zonal derivative of

<sup>1</sup>Center for Remote Sensing of the Earth (CERSE), Rome, Italy. <sup>2</sup>NATO STO-CMRE-Centre for Maritime Research and Experimentation, La Spezia, Italy.

✉email: luca\_borzelli@yahoo.it

the meridional mean between 5°S and 5°N of the wind velocity zonal component is minimum and identify the EWCZ longitude by fitting the meridional mean of the zonal wind profile with a step function. By using this concept, we show that internal downwelling waves, observed as intrusions in to the interior of the water column (i.e., between 50 and 250 m) of waters of surface origin, are regularly formed under the EWCZ, whose zonal displacements are strictly in phase with the Southern Oscillation Index (SOI); when the zonal position of the EWCZ moves further east than approximately 175°E, KWs formed beneath the EWCZ reach the eastern Pacific boundary and determine an El Niño event, which is more severe the more the EWCZ elongates into the interior of the tropical Pacific. Actually, observational studies<sup>32–34</sup> have demonstrated that WW events extend eastward in the tropical Pacific prior to an El Niño event and Lengaigne et al.<sup>35</sup> showed that the response of the ocean to these events is primarily characterized by a rapid eastward displacement of the WP. In a subsequent research, Lengaigne et al.<sup>36</sup> studied the response of the atmosphere to eastward displacements of the WP during the 1997/98 El Niño and demonstrated that these displacements induced eastward shifts of the deep atmospheric convection zone. Here we document that the region of deep atmospheric convection and the EWCZ displace zonally in phase with the SOI. Therefore, our results, along with the results published in the quoted literature, suggest that the role of WW events in the preconditioning phase of El Niño is twofold: on the one hand, WW events determine the convergence that triggers downwelling internal waves necessary to activate El Niño; and, on the other hand, they contribute in pushing eastward the WP and the region of deep atmospheric convection and, in this way, displace eastward the EWCZ in a region of the tropical Pacific where the process of mutual annihilation of KW and RW described by Kang and An<sup>24</sup> does not take place, creating the favorable condition for El Niño to develop.

## RESULTS AND DISCUSSION

In Fig. 1a we show the 6-month median filtered values of SOI and of the longitude of the EWCZ in the period Jan 1979–Aug 2019. Note that SOI is defined as the standardized differential surface pressure between Tahiti and Darwin (Australia): large positive SOI values are associated with increased EW (here the coordinate system is chosen so as that winds directed eastward are positive), while large negative values of SOI indicate enhanced WW and weakened EW. Therefore, the large negative Pearson correlation coefficient ( $\sim -0.9$ ) between the longitude of the EWCZ and SOI is not surprising and confirms the findings of other authors. Specifically, Lengaigne et al.<sup>35</sup>, using a general circulation model to study the evolution of the tropical Pacific during the 1997/98 El Niño, showed that the response of the ocean to WW events was characterized by a cooling of the western Pacific and an eastward displacement of the WP. In a subsequent study, Lengaigne et al.<sup>36</sup> demonstrated that these oceanic effects promoted the occurrence of a low-pressure system over the central Pacific, the weakening of EW and further, more intense and located more eastward, WW events. The large correlation between EWCZ position and SOI, however, demonstrates that the relationship between changes in the large-scale pressure system over the central Pacific, zonal position of WW events, and EW variability not only relates to the 1997/98 El Niño episode, but it is a characteristic of the tropical Pacific climate system. Furthermore, because of their short time scale, WW events have been often considered a stochastic forcing of El Niño, independent of the interannual variability of the tropical Pacific. However, some authors<sup>37,38</sup> proposed that the occurrence and characteristics of WW events depend on the state of El Niño and Hong and Jin<sup>39</sup> and Sullivan et al.<sup>40</sup> showed that WW events can be associated with the occurrence of a high-pressure system over the Australian monsoon region (Darwin). The

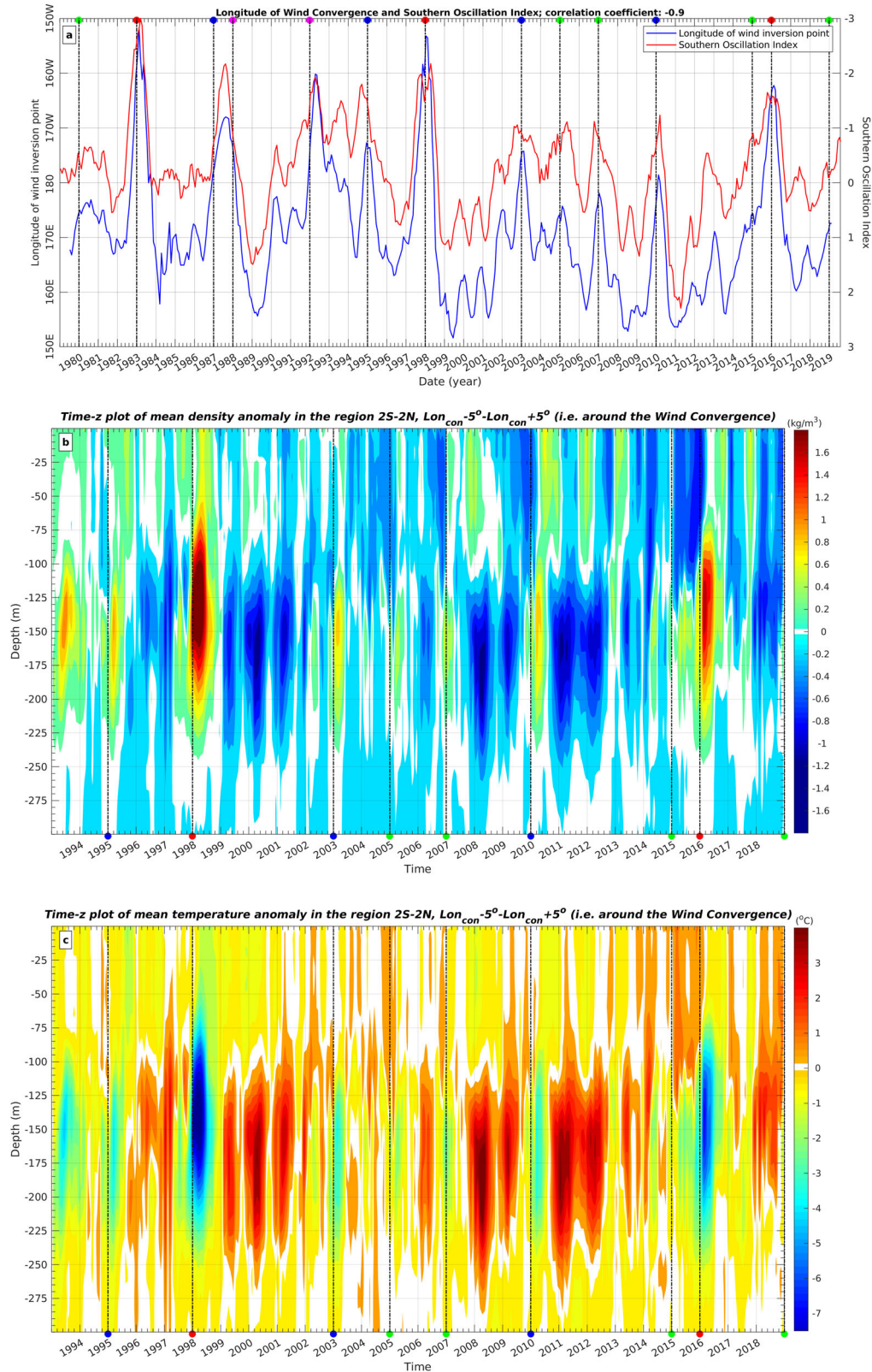
large correlation between SOI and the zonal position of the EWCZ confirms that WW events are modulated by the climate state of tropical Pacific region and are associated with large-scale changes of the pressure system over the region.

Figure 1b shows the time-z plot of the ocean water density anomaly averaged over a region centered below the EWCZ and extending 10° zonally and 4° meridionally. Figure 1c shows the time-z plot of the ocean water temperature anomaly averaged over the same region. Figure 2a shows the daily variability in the meridional mean of the zonal wind averaged west and east of the EWCZ: west of the convergence, the zonal wind oscillates around zero with values comprised between  $-4 \text{ m} \cdot \text{s}^{-1}$  (negative winds are directed westward) and  $3 \text{ m} \cdot \text{s}^{-1}$  (positive winds are directed eastward); east of the convergence, the zonal wind is always directed westward with values between  $-5.5 \text{ m} \cdot \text{s}^{-1}$  and  $-0.5 \text{ m} \cdot \text{s}^{-1}$ . In Fig. 2b the east/west difference in the zonal wind is represented and shows that, except for three cases in May/June 1983, 1984, and 1998, it is always negative, indicating that the flow associated with zonal winds is predominantly convergent. Comparing Figs. 1b, 2, it is therefore clear that the wind convergence, before an El Niño event, systematically pushes downward, towards the interior of the water column, waters less dense than normal; after the El Niño peaks, the convergence loosens (Fig. 2b) and the interior of the water column is replenished by denser waters (Fig. 1b).

Figure 3 shows the KW amplitude extracted from sea surface height (SSH) data and, superimposed on the image, the longitude of the EWCZ. As it is clear from the inspection of Fig. 3, KWs form regularly below the wind convergence, but only when the wind convergence is east of, approximately, 175°E does the resulting KW reach the eastern Pacific boundary and an El Niño event is recorded. Eastward shift of the KW formation region is also confirmed by a preliminary analysis of the depth of the 20°C isotherm provided by the Global Tropical Moored Buoy Array (<https://www.pmel.noaa.gov/tao/drupal/disdel/>). Furthermore, the further eastwards the wind convergence zone reaches into the central Pacific, the greater is the severity of the El Niño event (see, for reference, El Niño events on the right vertical axis of Fig. 3). This phenomenon is important and, since it indicates that the position of the wind convergence plays a key role in the El Niño initiation and intensity, warrants further discussion. Following Kang and An<sup>24</sup>, the KWs and RWs contributions to changes in the thermocline depth cancel each other in the western equatorial Pacific (i.e. west of 170°E). So, when the EWCZ is located west of 170°E, the resulting RWs and KWs interfere with each other destructively and do not determine changes in the thermocline depth. East of approximately 170°E the thermocline starts sloping (e.g.<sup>41,42</sup>) and, when RWs and KWs are excited in this region, RWs, to conserve potential vorticity, deviate poleward, leave the equatorial belt and stop interacting with KWs<sup>43</sup> that are left acting to modify efficiently the depth of the thermocline. This reasoning provides a reasonable explanation on why only when the wind convergence zone is further east than approximately 175°E an El Niño event is recorded.

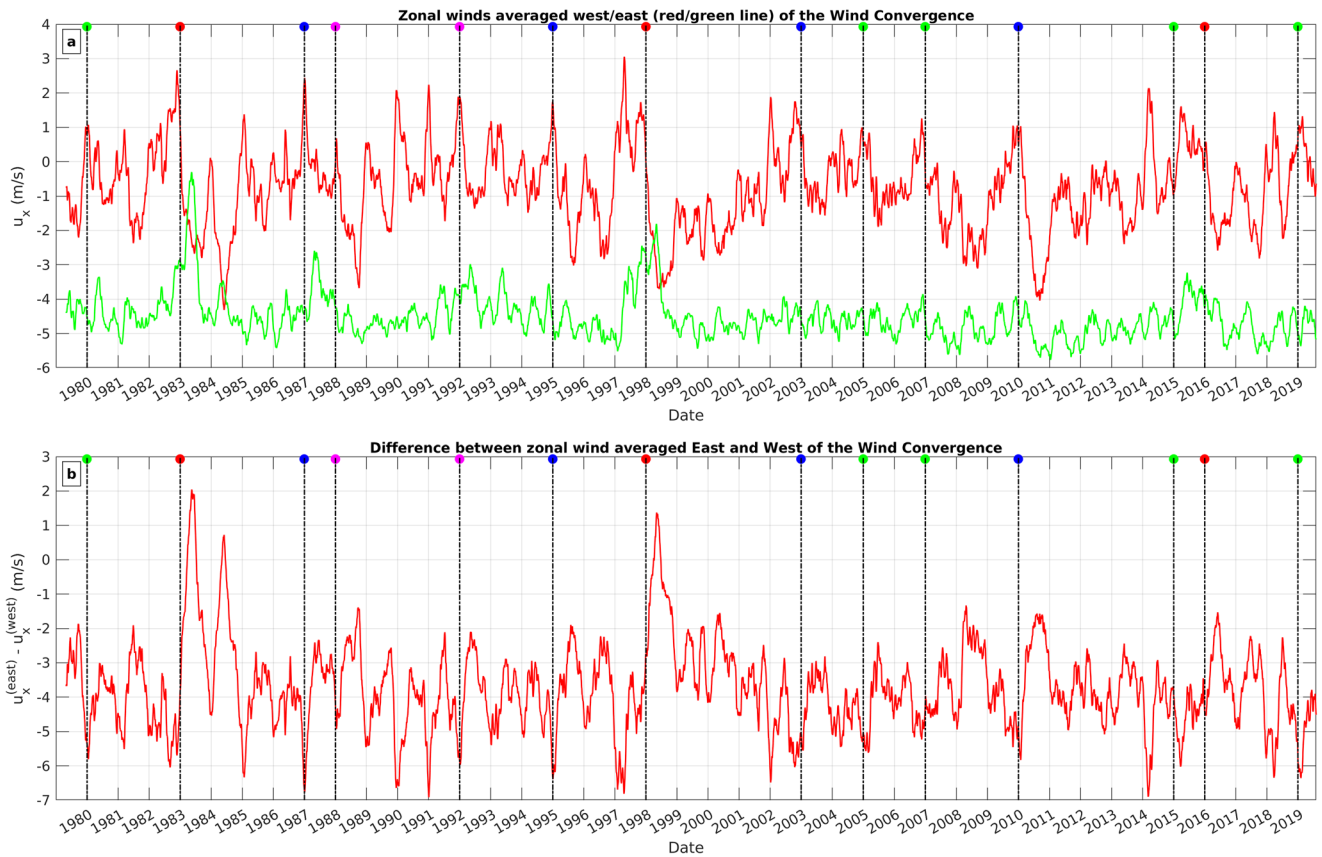
Another important feature described by Fig. 3 relates the 2014 “false” El Niño alarm; in early 2014, most dynamic forecast models predicted a developing strong El Niño. However, this much-anticipated event failed to materialize, whereas an unforeseen strong El Niño developed in 2015<sup>28–31</sup>. Indeed, from Fig. 3 we can see that during 2014 a KW propagates across the entire tropical Pacific, but the EWCZ remains to the west of 175°E, confirming that according to the theory proposed in this manuscript this would turn out to be a non-event. Conversely, in 2015 the EWCZ intruded deeply in to the central/eastern tropical Pacific and a super El Niño event developed.

Figure 4a shows zonal displacements of the point of maximum vertical atmospheric convection and, for the reader convenience, again as in Fig. 1a, the SOI. Also in this case, the data sets are



**Fig. 1** SOI, EWCZ and internal waves generation. **a** Longitude of wind reversal point (blue line) and SOI (red line). Left vertical axis refers to longitudes of wind reversal point; SOI values are reported on the right vertical axis. Colored points on the top of the horizontal axis represent El Niño events obtained from <https://ggweather.com/enso/oni.htm>. Color of the points represent El Niño event intensity, with the following legend: red, very strong; magenta, strong; blue, moderate; green, weak. **b** Time-z plot of sea water density anomaly. **c** Time-z plot of temperature anomaly. On the bottom horizontal axis of (**b**) and (**c**), points represent El Niño events classified with the same color legend of **a**.





**Fig. 2** Average winds east and west of the convergence. **a** Meridional mean between  $5^{\circ}\text{S}$  and  $5^{\circ}\text{N}$  of the daily zonal wind averaged west (red line) and east (green line) of the convergence point. **b** Winds to the west of EWCZ minus winds to the east (i.e., red line minus green line in (a)). In both panels, colored points represent El Niño events classified as discussed in the legend of Fig. 1a.

rather well correlated (correlation coefficient  $\sim -0.6$ ). Figure 4b shows the time-longitude plot of the surface wind vertical component and, as in Fig. 1b, superimposed on the image, the longitude of the EWCZ. The relationships between SOI, displacements of the atmospheric convection and zonal shifts of the EWCZ are coherent with the discussion of Fig. 1 and confirm observations and modeling published in the available literature. Indeed, Picaut et al.<sup>18</sup> observed that zonal displacements of the WP are well correlated to SOI and Lengaigne et al.<sup>35,36</sup> demonstrated that, during the 1997/98 El Niño, the response of the tropical Pacific climate system was characterized by an eastward shift of the WP and, consequently, an eastward shift of the atmospheric convection. Here we find that SOI and zonal shifts of atmospheric convection are, indeed, correlated. Since the zonal displacements of the atmospheric convection zone and of the EWCZ are correlated (because both are correlated to SOI), our results naturally confirm that WW events are modulated by the state of El Niño<sup>38</sup>, but, more generally, show that WW events are modulated by the state of the tropical Pacific ocean-atmosphere climate system.

In this paper we have discussed El Niño initiation in relation to westerly wind forcing and internal wave generation from a slightly different perspective to that commonly adopted. Specifically, we have seen that westerly wind events are RW and KW generators in the sense that their encounter with the nearly stationary trade winds determines a convergence and, therefore, the conditions necessary to excite the waves. However, only when the Easterlies/Westerlies convergence occurs east of  $175^{\circ}\text{E}$ , is an El Niño event effectively initiated. We have explained this phenomenon in terms of mutual annihilation of KWs and RWs propagating over a flat interface and deviations towards the poles of RWs propagating

over a sloping interface, which, consequently, east of  $175^{\circ}\text{E}$ , where the thermocline starts sloping, exit from the equatorial belt and stop interacting with equatorial KWs. In this context, we have emphasized the importance of the position of the Easterlies/Westerlies convergence and shown that it is correlated with the SOI. This suggests that westerly wind events are part of the tropical Pacific climate system and, indeed, we found that lateral shifts of the atmospheric convection, changes in the large scale zonal sea level pressure gradient, zonal displacements of the Easterlies/Westerlies convergence zone take place in phase. These results, along with the fact that zonal displacements of the WP occur in phase with the SOI<sup>18</sup>, beside defining a synthetic parameter that describes favorable conditions for El Niño onset (i.e., the eastward extension of the easterlies/westerlies wind convergence), provide a description of the tropical Pacific climate system in which El Niño is the logical consequence. Indeed, the competition between westerly wind events and Easterlies determines zonal shifts of the WP, triggering the position of the deep atmospheric convection. However, zonal displacements of the deep convection determine changes in the tropical Pacific pressure system and, consequently, determine changes in the intensity of westerly wind events and zonal displacements of the Easterlies/Westerlies convergence zone. When the position of the Easterlies/Westerlies convergence reaches  $175^{\circ}\text{E}$  the thermocline starts sloping, KWs and RWs are formed over the sloping thermocline and an El Niño event is recorded.

As a final remark, under the influence of global greenhouse warming, the mean climate of the Pacific region will undergo significant changes. Specifically, projections involve weakening of the trade winds, changes in the thermocline depth<sup>44</sup>, decrease of the zonal sea surface temperature gradients and more intense and



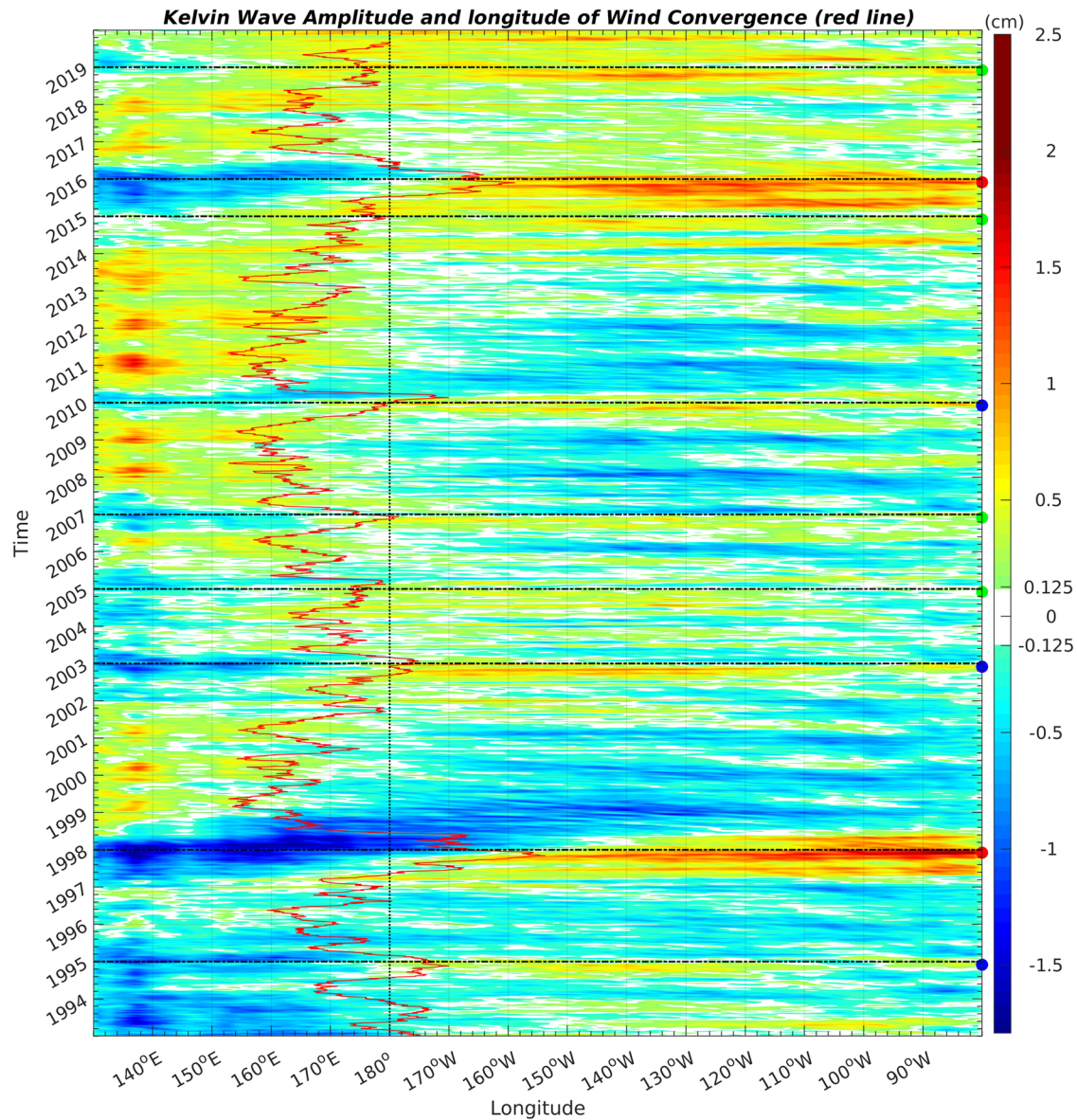


**Fig. 3** Daily Kelvin wave amplitude and, superimposed on the image, the red line representing the longitude of the wind convergence computed from daily wind data. On the right vertical axis, points represent El Niño events classified with the same color legend of Fig. 1a.

frequent El Niño episodes<sup>45</sup>. We believe that the results presented here offer valuable insights on assessing possible future shifts of ENSO regimes, including useful considerations related to the climate change and security nexus. It is our intention to carry out research with the aim of estimating long-term changes in the position of the Easterlies/Westerlies convergence zone and in the shape of isothermal surfaces that can explain changes in the characteristics of El Niño episodes.

## METHODS

Wind data are the zonal, meridional and vertical component of monthly winds provided by the ERA-Interim project and zonal component of daily winds obtained by daily averaging 6-hourly surface analysis of the ERA-Interim, covering the period 1 Jan 1979–31 Aug 2019 over the region 130°E–80°W, 5°S–5°N. Both data sets were extracted from the Research Data Archive at the National Center for Atmospheric Research - USA (prod. #627.1 and #627.2, respectively). The longitude of the EWCZ was determined by fitting, in the zonal region 130°E–100°W, in every date of the

observation period, the meridional mean of the zonal wind with a step function. In practice, the longitudinal segment of the observation domain was divided into two sub-segments of varying length; average values of the meridional means of zonal wind were computed for each segment to obtain a set of step function representations of the meridional means of the zonal wind. Among the different representations, the one that minimized the root-mean-square between itself and the original meridional mean was chosen as the best step function representation of the zonal wind. SOI data were downloaded from the Climatic Research Unit at the University of East Anglia – UK.

To detect propagating KWs, daily Sea Surface Height (SSH) data with spatial resolution of 0.25° × 0.25° provided by orbiting altimeters over the region 15°S–15°N, 130°E–80°W in the period 1 Jan 1993–31 Dec 2019 and processed by the Copernicus European Marine Service (prod. SEALEVEL\_GLO\_PHY\_L4\_MY\_008\_047), were re-sampled weekly using a cubic spline. Following Boulanger and Menkes<sup>46,47</sup> and Boulanger et al.<sup>48</sup>, KW amplitudes were computed by expressing the SSH

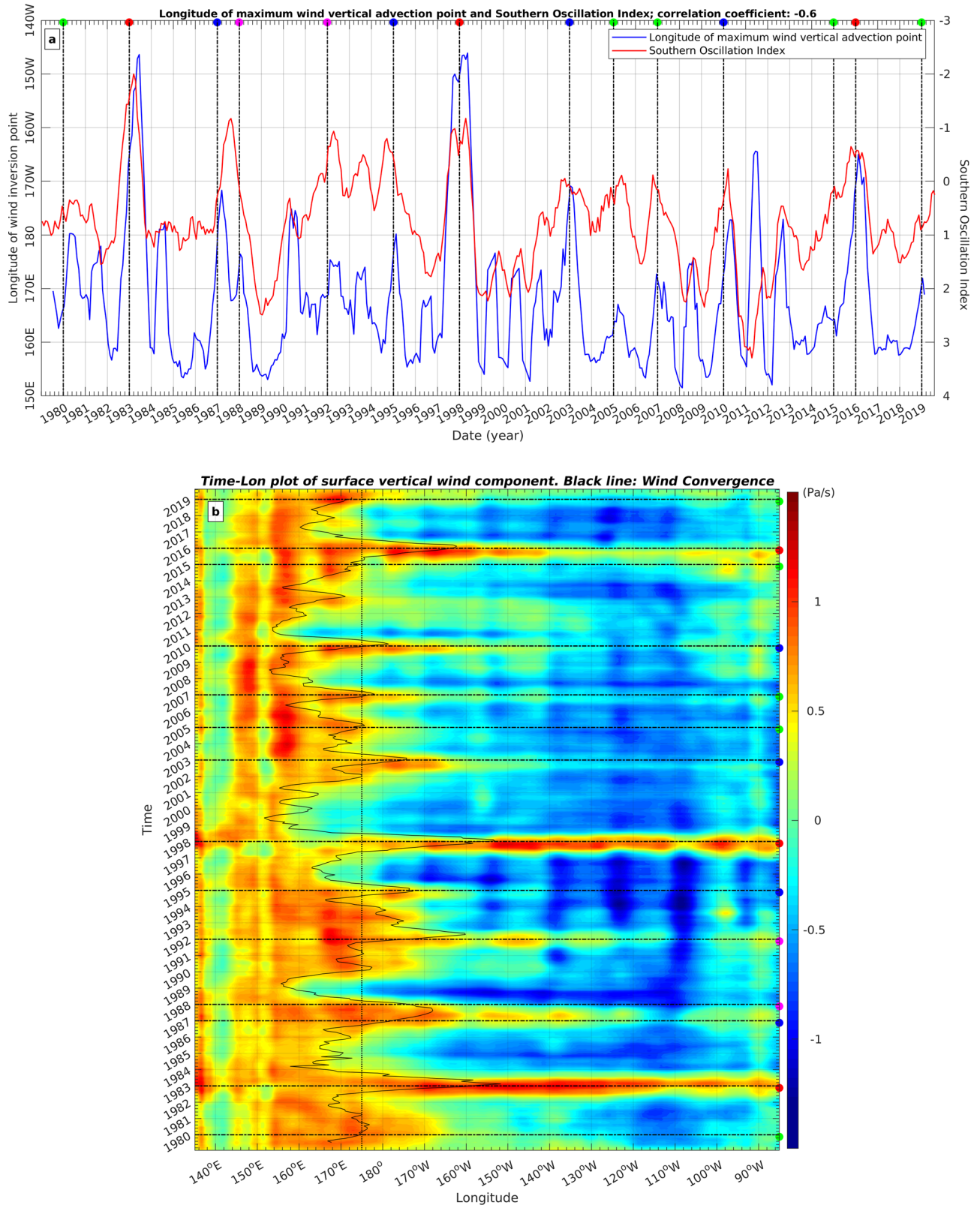


**Fig. 4** SOI, atmospheric convection and EWCZ. **a** Longitude of maximum wind vertical advection (blue line) and SOI (red line). Left vertical axis refers to longitudes of the point of the maximum wind vertical advection; SOI values are reported on the right vertical axis. Colored points on top horizontal axis, represent El Niño events classified as discussed in the legend of Fig. 1a. **b** Longitude-time plot of the wind vertical advection, the black line represents the longitude of the wind convergence. Colored points on the right vertical axis represent El Niño events classified as discussed in the legend of Fig. 1a.



( $\eta$ ) as a linear superposition of freely propagating RWs and KWs, namely

$$\eta(x, y, t) = \sum_{n=0}^{\infty} r_n(x, t) \cdot R_n \left( y \sqrt{\frac{\beta}{2c}} \right) \quad (1)$$

where  $r_0$  is the KW amplitude,  $R_n$  ( $n = 1, 2, \dots$ ) are functions related to the parabolic cylinder functions and  $c$  was set to  $2.5 \text{ m} \cdot \text{s}^{-1}$  (for details on the derivation, see ref. <sup>46</sup>, Appendix A1, and <sup>49</sup>, page 454).

Monthly, in situ Temperature-Salinity (TS) data sampled on a regular spatial grid of  $0.25^\circ \times 0.25^\circ$ , over 50 vertical levels (from 0 to 5500 m), covering the region  $15^\circ\text{S}$ – $15^\circ\text{N}$   $130^\circ\text{E}$ – $80^\circ\text{W}$  in the period 16 Jan 1993–16 Dec 2018, were provided by the Copernicus Marine Environment Monitoring Service of the European Union (prod. MULTIOBS\_GLO\_PHY\_TSUV\_3D\_MYNRT\_015\_012, data set: armor-3d-rep-monthly) and used to compute sea water density profiles ( $\rho(x, y, z, t)$ ) using the CSIRO library of MATLAB computational routines for the properties of sea water<sup>50</sup>.

## DATA AVAILABILITY

Data used in this research can be downloaded succumbing to European Union (EU) regulations on geophysical data exchange (see <https://eur-lex.europa.eu/legal-content/EN/TXT/?uri=celex%3A32014R0377>). Original Sea Surface Height (SSH) and TS data are processed and distributed in NetCDF to registered users by the Copernicus European Marine Service at the following web site: [https://resources.marine.copernicus.eu/product-detail/SEALEVEL\\_GLO\\_PHY\\_L4\\_MY\\_008\\_047/INFORMATION](https://resources.marine.copernicus.eu/product-detail/SEALEVEL_GLO_PHY_L4_MY_008_047/INFORMATION). [https://resources.marine.copernicus.eu/product-detail/MULTIOBS\\_GLO\\_PHY\\_TSUV\\_3D\\_MYNRT\\_015\\_012/INFORMATION](https://resources.marine.copernicus.eu/product-detail/MULTIOBS_GLO_PHY_TSUV_3D_MYNRT_015_012/INFORMATION). Original wind data are monthly means and 6-hourly surface analysis data of the ERA-Interim project distributed by the National Center for Atmospheric Research (NCAR)-Research Data Archive (prod. #627.1 and #627.2, doi: 10.5065/D68050NT) and can be downloaded by registered users in NetCDF from: <https://rda.ucar.edu/datasets/ds627.1/>. <https://rda.ucar.edu/datasets/ds627.2/>. Southern Oscillation Index data have been downloaded from the Climatic Research Unit at the University of East Anglia – UK and can be downloaded at: <https://crudata.uea.ac.uk/cru/data/soi/soi.dat>. The T-S, SSH and zonal wind data sets over the region under study and the Southern Oscillation Index data in Matlab format used in this study (<https://doi.org/10.6084/m9.figshare.23779860>) can be downloaded by users registered to the FigShare.com service at the following web site: [https://figshare.com/articles/dataset/T-S\\_almimeter\\_zonal\\_wind\\_data\\_sets\\_over\\_the\\_Tropical\\_Pacific\\_and\\_software\\_used\\_in\\_Eusebi\\_Borzelli\\_and\\_Carniel\\_2023\\_-\\_Where\\_the\\_winds\\_clash\\_what\\_is\\_really\\_triggering\\_El\\_Ni\\_o\\_initiation\\_npj\\_Climate\\_and\\_Atmos\\_Sci\\_/23779860](https://figshare.com/articles/dataset/T-S_almimeter_zonal_wind_data_sets_over_the_Tropical_Pacific_and_software_used_in_Eusebi_Borzelli_and_Carniel_2023_-_Where_the_winds_clash_what_is_really_triggering_El_Ni_o_initiation_npj_Climate_and_Atmos_Sci_/23779860). The datasets used in this research are also available from the corresponding author on reasonable request.

## CODE AVAILABILITY

Program and scripts especially developed for this study under Unix platform (Ubuntu Release 18.4.5 LTS) in MATLAB R2018a environment (<https://doi.org/10.6084/m9.figshare.23779860>) can be downloaded by users registered to the FigShare.com service at the following web site: [https://figshare.com/articles/dataset/T-S\\_almimeter\\_zonal\\_wind\\_data\\_sets\\_over\\_the\\_Tropical\\_Pacific\\_and\\_software\\_used\\_in\\_Eusebi\\_Borzelli\\_and\\_Carniel\\_2023\\_-\\_Where\\_the\\_winds\\_clash\\_what\\_is\\_really\\_triggering\\_El\\_Ni\\_o\\_initiation\\_npj\\_Climate\\_and\\_Atmos\\_Sci\\_/23779860](https://figshare.com/articles/dataset/T-S_almimeter_zonal_wind_data_sets_over_the_Tropical_Pacific_and_software_used_in_Eusebi_Borzelli_and_Carniel_2023_-_Where_the_winds_clash_what_is_really_triggering_El_Ni_o_initiation_npj_Climate_and_Atmos_Sci_/23779860). Software developed for the current study is also available from the corresponding author on reasonable request.

Received: 22 March 2023; Accepted: 3 August 2023;

Published online: 18 August 2023

## REFERENCES

- Philander, S. G. H. *El Nino, La Nina and the Southern Oscillation* (Academic Press, 1990).
- Santoso, A., McPhaden, M. J. & Cai, W. The defining characteristics of ENSO extremes and the strong 2015/2016 El Niño. *Rev. Geophys.* **55**, 1079–1129 (2017).
- Wang, C. A review of ENSO theories. *Natl Sci. Rev.* **5**, 813–825 (2018).
- Holbrook, N. J. et al. ENSO-Driven Ocean Extremes and Their Ecosystem Impacts, *El Niño southern oscillation in a changing climate*, 409–428. <https://doi.org/10.1002/9781119548164.ch18> (2020).
- McPhaden, M. J., Zebiak, S. E. & Glantz, M. H. (2006). ENSO as an integrating concept in earth science. *Science* **314**, 1740–1745 (2006).
- Iizumi, T. et al. Impacts of El Niño Southern Oscillation on the global yields of major crops. *Nat. Commun.* **5**, 3712 (2014).
- Roy, S. S. Role of ENSO on Conflicts in the Global South. *Front. Clim.* **4**, 7 (2022).
- Wang, Q. et al. Quantifying the influence of climate variability on armed conflict in Africa, 2000–2015. *Environ. Dev. Sustain.* <https://doi.org/10.1007/s10668-022-02436-x> (2022).
- Wyrtki, K. El Niño—The dynamic response of the equatorial Pacific Ocean to atmospheric forcing. *J. Phys. Oceanogr.* **5**, 572–584 (1975).
- Jin, F.-F. An equatorial ocean recharge paradigm for ENSO. Part I: Conceptual model. *J. Atmos. Sci.* **54**, 811–829 (1997).
- Burgers, G. & Jin, F.-F. The simplest ENSO recharge oscillator. *Geophys. Res. Lett.* **32**, 13 (2005).
- Wyrtki, K. Some thoughts about the west Pacific Warm Pool. Paper presented at West Pacific Int. Meeting and Workshop on TOGA COARE, ORSTOM, Nouméa, New Calédonia (1989).
- Picaut, J. & Delcroix, T. Equatorial wave sequence associated with warm pool displacements during the 1986–1989 El Niño–La Niña. *J. Geophys. Res.* **100**, 18393–18408 (1995).
- Mignot, J., de Boyer Montégut, C., Lazar, A. & Cravatte, S. Control of salinity on the mixed layer depth in the world ocean: 2. Tropical areas. *J. Geophys. Res.* <https://doi.org/10.1029/2006JC003954> (2007).
- Cravatte, S., Delcroix, T., Zhang, D., McPhaden, M. & Leloup, J. Observed freshening and warming of the western Pacific warm pool. *Clim. Dyn.* **33**, 565–589 (2009).
- Kim, S. T., Yu, J. Y. & Lu, M. M. The distinct behaviors of Pacific and Indian Ocean warm pool properties on seasonal and interannual time scales. *J. Geophys. Res.* <https://doi.org/10.1029/2011JD016557> (2012).
- De Deckker, P. The Indo-Pacific Warm Pool: critical to world oceanography and world climate. *Geosci. Lett.* **3**, 20 (2016).
- Picaut, J., Ioualalen, M., Menkès, C., Delcroix, T. & McPhaden, M. J. Mechanism of the zonal displacements of the Pacific warm pool: Implications for ENSO. *Science* **274**, 1486–1489 (1996).
- Delcroix, T. & Picaut, J. Zonal displacement of the western equatorial Pacific “fresh pool”. *J. Geophys. Res.* **103**, 1087–1098 (1998).
- Picaut, J. et al. The oceanic zone of convergence on the eastern edge of the Pacific warm pool: a synthesis of results and implications for El Niño–Southern Oscillation and biogeochemical phenomena. *J. Geophys. Res.* **106**, 2363–2386 (2001).
- Delcroix, T. & McPhaden, M. Interannual sea surface salinity and temperature changes in the western Pacific warm pool during 1992–2000. *J. Geophys. Res.* **107**, SRF 3-1–SRF 3-17 (2002).
- Ashafahani, A. A., Wirasatriya, A., Pranowo, W. S., Sugianto, D. N. & Maslukah, L. The Dynamic of Convergence Zone Displacement in Western Pacific Ocean on 2015 Super El Niño Event. *IOP Conf. Ser.: Earth Environ. Sci.* **750**, 1 (2021).
- Sun, C. et al. Cross-hemispheric SST propagation enhances the predictability of tropical western Pacific climate. *NPJ Clim. Atmos.* **5**, 38 (2022).
- Kang, I. S. & An, S. I. Kelvin and Rossby wave contributions to the SST oscillation of ENSO. *J. Clim.* **11**, 2461–2469 (1998).
- Hayashi, M. & Watanabe, M. Importance of background seasonality over the eastern equatorial Pacific in a coupled atmosphere–ocean response to westerly wind events. *Clim. Dyn.* **52**, 7309–7327 (2019).
- Yu, S. & Fedorov, A. V. The role of westerly wind bursts during different seasons versus ocean heat recharge in the development of extreme El Niño in climate models. *Geophys. Res. Lett.* **47**, 16 (2020).
- Yu, S. & Fedorov, A. V. The Essential Role of Westerly Wind Bursts in ENSO Dynamics and Extreme Events Quantified in Model “Wind Stress Shaving” Experiments. *J. Clim.* **35**, 7519–7538 (2022).
- McPhaden, M. J. Playing hide and seek with El Niño. *Nat. Clim. Change* **5**, 791–795 (2015).
- McPhaden, M. J., Timmermann, A., Widlansky, M. J., Balmaseda, M. A. & Stockdale, T. N. The curious case of the El Niño that never happened: a perspective from 40 years of progress in climate research and forecasting. *Bull. Am. Meteorol. Soc.* **96**, 1647–1665 (2015).
- Hu, S. & Fedorov, A. V. Exceptionally strong easterly wind burst stalling El Niño of 2014. *Proc. Natl Acad. Sci. USA* **113**, 2005–2010 (2016).
- Levine, A. F. Z. & McPhaden, M. J. How the July 2014 easterly wind burst gave the 2015–2016 El Niño a head start. *Geophys. Res. Lett.* **43**, 6503–6510 (2016).
- Harrison, D. E. & Vecchi, G. A. Westerly wind events in the tropical Pacific, 1986–95. *J. Clim.* **10**, 3131–3156 (1997).
- McPhaden, M. J. Climate oscillations: Genesis and evolution of the 1997–98 El Niño. *Science* **283**, 950–954 (1999).
- Vecchi, G. & Harrison, D. Tropical Pacific sea surface temperature anomalies, El Niño, and equatorial westerly wind events. *J. Clim.* **13**, 1814–1830 (2000).



35. Lengaigne, M. et al. Ocean response to the March 1997 Westerly Wind Event. *J. Geophys. Res.* **107**, SRF 16-1–SRF 16-20 (2002).
36. Lengaigne, M. et al. The March 1997 Westerly Wind Event and the Onset of the 1997/98 El Niño: understanding the role of the atmospheric response. *J. Clim.* **16**, 3330–33432 (2003).
37. Lengaigne, M. et al. Triggering of El Niño by westerly wind events in a coupled general circulation model. *Clim. Dyn.* **23**, 601–620 (2004).
38. Eisenman, I., Yu, L. & Tziperman, E. Westerly wind bursts: ENSO's tail rather than the dog? *J. Clim.* **18**, 5224–5238 (2005).
39. Hong, L.-C. H. L. & Jin, F.-F. A southern hemisphere booster of super El Niño. *Geophys. Res. Lett.* **410**, 2142–2149 (2014).
40. Sullivan, A. et al. Generation of westerly wind bursts by forcing outside the tropics. *Sci. Rep.* **11**, 912 (2021).
41. Yang, H. & Wang, F. Revisiting the thermocline depth in the equatorial Pacific. *J. Clim.* **22**, 3856–3863 (2009).
42. Castaño-Tierno, A., Mohino, E., Rodríguez-Fonseca, B. & Losada, T. Revisiting the CMIP5 Thermocline in the Equatorial Pacific and Atlantic Oceans. *Geophys. Res. Lett.* **45**, 12963–12971 (2018).
43. Yang, J. & Yu, L. Propagation of equatorially trapped waves on a sloping thermocline. *J. Phys. Oceanogr.* **22**, 573–582 (1992).
44. Collins, M. et al. The impact of global warming on the tropical Pacific Ocean and El Niño. *Nat. Geosci.* **3**, 391–397 (2010).
45. Cai, W. et al. Changing El Niño-Southern Oscillation in a warming climate. *Nat. Rev. Earth Environ.* **2**, 628–644 (2021).
46. Boulanger, J. P. & Menkes, C. Propagation and reflection of long equatorial waves in the Pacific Ocean during the 1992–1993 El Niño. *J. Geophys. Res.* **100**, 25041–25059 (1995).
47. Boulanger, J. P. & Menkes, C. Long equatorial wave reflection in the Pacific Ocean from TOPEX/POSEIDON data during the 1992–1998 period. *Clim. Dyn.* **15**, 205–225 (1999).
48. Boulanger, J. P., Cravatte, S. & Menkes, C. Reflected and locally wind-forced interannual equatorial Kelvin waves in the western Pacific Ocean. *J. Geophys. Res.* <https://doi.org/10.1029/2002JC001760> (2003).
49. Gill, A. E. *Atmosphere-ocean Dynamics* (Academic Press 1982).
50. Morgan, P. P. SEAWATER: a library of MATLAB® computational routines for the properties of sea water: Version 1.2. Report No.:222. <http://hdl.handle.net/102.100.100/239771?index=1> (1994).

## ACKNOWLEDGEMENTS

Financial support from the Office of the NATO Chief Scientist is greatly acknowledged.

## AUTHOR CONTRIBUTIONS

G.L.E.B. and S.C. contributed equally to the work, by proposing the original idea and designing the research. Both authors analyzed the data and provided the figures. Both authors contributed in interpreting the results. G.L.E.B. wrote the initial version of the manuscript and S.C. provided corrections and comments.

## COMPETING INTERESTS

The authors declare no competing interests.

## ADDITIONAL INFORMATION

**Correspondence** and requests for materials should be addressed to Gian Luca Eusebi Borzelli.

**Reprints and permission information** is available at <http://www.nature.com/reprints>

**Publisher's note** Springer Nature remains neutral with regard to jurisdictional claims in published maps and institutional affiliations.



**Open Access** This article is licensed under a Creative Commons Attribution 4.0 International License, which permits use, sharing, adaptation, distribution and reproduction in any medium or format, as long as you give appropriate credit to the original author(s) and the source, provide a link to the Creative Commons license, and indicate if changes were made. The images or other third party material in this article are included in the article's Creative Commons license, unless indicated otherwise in a credit line to the material. If material is not included in the article's Creative Commons license and your intended use is not permitted by statutory regulation or exceeds the permitted use, you will need to obtain permission directly from the copyright holder. To view a copy of this license, visit <http://creativecommons.org/licenses/by/4.0/>.

© The Author(s) 2023